Proximate Time-Optimal Control of a Second-Order Flexible Structure

Roger A. Braker and Lucy Y. Pao

***Abstract*— We develop a Proximate Time-Optimal Servomechanism (PTOS) for a harmonic oscillator plant with no damping. We approximate the signum function inherent to the bang-bang, time-optimal solution with a gain and saturator. We prove that if certain design restrictions are met, this control law will drive any initial state into an invariant region $\mathcal{B}$ about the origin of the phase-plane in finite-time. We then show that once the state enters this region, it is asymptotically stable about the origin, by demonstrating that a Lyapunov function exists for the region $\mathcal{B}$. Finally, we present simulation results using this control law on a simplified model of an atomic force microscope.**

I. Introduction

The traditional Atomic-Force-Microscope (AFM) imaging method is to raster scan the sample with an atomically sharp probe. Raster scanning is not only a very time consuming process, it can also lead to damaging either the sample or the AFM probe tip or both. Traditionally, efforts to increase imaging speed have focused on increasing the raster scan rate via advanced control algorithms [1], [2].

Recently, a novel approach to AFM imaging has been suggested [3] whereby a random sample of point-to-point measurements are taken. The sample topology is then reconstructed using the theory of compressed sensing [4]. Taking this random sample of point-to-point measurements reduces the tip-sample interaction and can improve the integrity of both the sample and AFM tip.

In order to minimize the imaging time, the rest-to-rest maneuver times from one point measurement to the next must be minimized. While the vertical z-direction dynamics of some AFMs can be approximated by a first-order model, the dynamics in the x and y-directions can typically be reduced only to an oscillatory second-order model as discussed in [3] and which can also be seen in the frequency response function of the AFM stage considered in [1]. Although the time-optimal control of first-order systems is well understood [5], the time-optimal control of oscillatory second-order systems is less well characterized and is still an area of research [6].

For a linear time-invariant system, Pontryagin's Maximal Principle leads to a time-optimal control that is bang-bang [5]. Excellent resources for synthesizing these controls as feedback control laws can be found in [7]–[9]. Unfortunately, the bang-bang feedback control is impractical. In any real control system, there will be process and measurement noise, uncertainty in the system parameters and imperfect actuators which will cause the control to chatter between its maximum and minimum value. Researchers have proposed several methods to combat this undesirable behavior for other systems. In [10], a robust control law for a double integrator plant is developed using sliding mode techniques. Other researchers have developed the Proximate Time-Optimal Servomechanism (PTOS) for a double integrator plant [11] and a triple integrator plant [12].

Reference [13] suggests pre-computing the time-optimal trajectory which is then tracked with a stabilizing trajectory tracking control law. At the end of this reference trajectory, an end-game control law is implemented to eliminate any final error. A downside to this method is it requires pre-computation of individual trajectories for each initial condition and target state.

In this paper, we take inspiration from the PTOS controllers developed in [11] and [12] to develop a similar controller, PTOSω, for second-order systems with purely complex eigenvalues for the regulator case. We note that this controller has limited direct practical value since we have ignored damping and our controller only drives the system to the origin. Nonetheless, since the structure of this problem differs significantly from the existing PTOS controllers, this work represents a first step towards developing a fully usable PTOS for systems with complex poles. Section II summarizes the time-optimal solution and its associated chattering problems. In Section III, we develop the PTOSω controller. We show in Sections IV through VII that this controller leads to a stable, closed-system. Finally, we present simulation results and conclusions in Sections VIII and IX.

II. Problem Formulation

Here, we review the time-optimal regulator problem for the simple harmonic oscillator with mass $m = \frac{1}{b_o}$, spring constant $\frac{1}{c} = \frac{\omega^2}{b_o}$, and no damping such that the system can be described in state space by

$$\begin{bmatrix}\dot{x}_1\\ \dot{x}_2\end{bmatrix} = \begin{bmatrix}0 & 1\\ -\omega^2 & 0\end{bmatrix}\begin{bmatrix}x_1\\ x_2\end{bmatrix} + Bu \tag{1}$$

where $B = \begin{bmatrix}0 & b_o\end{bmatrix}^T$. The position is x_1 and the velocity is x_2. The input is bounded, $u(t) \in [-1, +1]$.

Problem: Given any initial state $x(0) = x_o$, transfer the system to the origin in minimal time.

The time-optimal solution can be derived from Pontryagin's Maximal Principle and it can be written as a feedback

This work was supported in part by the US National Science Foundation (NSF Grant CMMI-1234980), a University of Colorado Engineering Dean's Graduate Assistantship, and Agilent Technologies, Inc.

R.A. Braker is a graduate student and L.Y. Pao is the Richard & Joy Dorf Professor; both are with the Dept. of Electrical, Computer, and Energy Engineering at the University of Colorado, Boulder, CO 80309, roger.braker@colorado.edu, pao@colorado.edu.

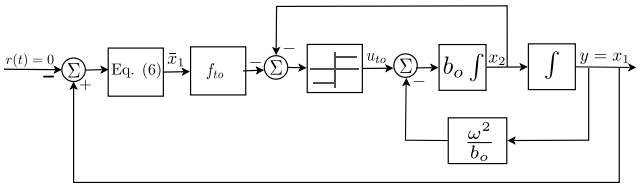

Fig. 1: Block diagram of time-optimal controller.

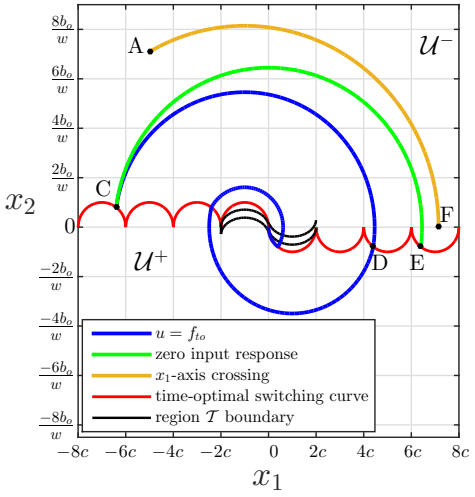

Fig. 2: The time-optimal switching curve (solid red) f_{to} divides $\mathbb{R}^2$ into $\mathcal{U}^+$and $\mathcal{U}^-$. Trajectory CE shows the state evolve with zero input. Compare this to the time-optimal trajectory CD, where the control has decreased the magnitude of x_1 by $2c$. The number of control switches from an initial state A to the PTOSω region is calculated by determining from (21) the first intercept with the x_1-axis, point F.

control law as [7]–[9]

$$u_{to}\left(\bar{x}_1, x_2\right)) = \text{sgn}\big(-x_2 - f_{to}(\bar{x}_1)\big) \tag{2}$$

$$f_{to}(\bar{x}_1) = \text{sgn}(\bar{x}_1)\omega\sqrt{c^2 - \bar{x}_1^2} \tag{3}$$

where the sgn$(\cdot)$ is defined as

$$\text{sgn}(\xi) = \begin{cases} +1, & \xi > 0 \\ 0, & \xi = 0 \\ -1, & \xi < 0 \end{cases}$$

and where $\bar{x}_1$ is given by

$$\bar{x}_1 = \begin{cases} \text{sgn}(x_1)\left[c - \text{frac}\left(\frac{|x_1|}{c}\right)c\right], & \lfloor \frac{|x_1|}{c} \rfloor \bmod 2 = 0 \\ \text{frac}(\frac{x_1}{c})c, & \text{otherwise} \end{cases} \tag{4}$$

where frac$(\cdot)$ yields the fractional remainder of its argument and $\lfloor(\cdot)\rfloor$ is the standard floor function. Noting the time dependence of x_1 and x_2, we will often simply write $u_{to}(t)$. Figure 1 shows a block diagram of the control scheme. We call $f_{to}(\bar{x}_1)$ the *switching curve*. Consisting of semi-ellipses, it divides the state space into two regions, $\mathcal{U}^+$ and $\mathcal{U}^-$, as shown by the red curve in Figure 2. The control is $u = -1$ when x_2 is above the switching curve, and $u = +1$ when x_2 is below the switching curve.

Although the control is optimal, it is impractical to implement on a real system. It is well known that a bang-bang feedback control leads to chatter in the presence of disturbances and model uncertainty and sensor noise [14]. This control law is no different. At the last switch, the state will ideally follow the switching curve to the origin, as in the blue trajectory in Figure 2. However, in practice, the control will chatter between -1 and $+1$ after this last switch.

III. Practical Near Time-Optimal Controller

The chatter problem of time-optimal control laws for a few other systems has been addressed by approximating the sgn$(\cdot)$ function with a saturator and a gain [11], [12]. We take a similar approach here in deriving the PTOSω for the system defined in (1). The saturator is defined as

$$\text{sat}(\xi) = \begin{cases} +1, & \xi > 1 \\ \xi, & |\xi| \le 1 \\ -1, & \xi < -1. \end{cases} \tag{5}$$

Since the time-optimal trajectory only attempts to follow the switching curve after the final switch, we only modify (2) and (3) when $|x_1| \le 2c$. In this region, we consider the controller given by

$$u_p(t) = \text{sat}\big[k_2(-x_2 - f_p(x_1))\big] \tag{6}$$

where $f_p(x_1)$ is defined later in (13).

In the rest of the paper, we will use the following divisions of the state space:

$$\mathcal{T} = \big\{x\colon |x_2 + f_p(x_1)| \le \frac{1}{k_2}, \quad x_1 \in [-2c, 2c]\big\} \tag{7}$$

$$\mathcal{B} = \big\{x\colon x \in \mathcal{T}, \quad x_1 \in [-c, c]\big\} \tag{8}$$

$$\mathcal{L} = \big\{x\colon x \in B, \quad x_1 \in [-x_\ell, x_\ell]\big\} \tag{9}$$

$$\mathcal{U}^- = \big\{x\colon x \notin \mathcal{T}, \quad x_2 > -f_p(x_1)\big\} \tag{10}$$

$$\mathcal{U}^+ = \big\{x\colon x \notin \mathcal{T}, \quad x_2 \le -f_p(x_1)\big\}. \tag{11}$$

Similar to their definition in the time-optimal case, $\mathcal{U}^-$ and $\mathcal{U}^+$ are the regions of $\mathbb{R}^2$ that result in a saturated control while $x \in \mathcal{T} \subset \mathbb{R}^2$ results in an unsaturated control. Furthermore, note that $\mathcal{B} \subset \mathcal{T}$ and $\mathcal{L} \subset \mathcal{B}$ while $\mathcal{U}^+ \cup \mathcal{T} \cup \mathcal{U}^- = \mathbb{R}^2$.

A. Development of $f_p(x_1)$

In this section, we focus our attention on the region in the state space where $|x_1| \le 2c$. Here, $f_{to}(\bar{x}_1)$ is equivalent to

$$f(x_1) = \text{sgn}(x_1)\omega\sqrt{2\alpha c|x_1| - \alpha x_1^2} \tag{12}$$

if $\alpha = 1$. In general, $0 < \alpha \le 1$ is a discount factor that ensures there is sufficient control authority left to account for modeling errors. We can combine a linear controller near the origin with a faster, more aggressive controller that approximates f_{to} "far" from the origin by defining f_p as the piecewise continuous function

$$f_p(x_1) = \begin{cases} f_\ell(x_1) & |x_1| \le x_\ell \\ f_{n\ell}(x_1) & x_\ell < |x_1| < 2c \\ f_{to}(\bar{x}_1) & \text{otherwise,} \end{cases} \tag{13}$$

where

$$f_\ell(x_1) = \frac{k_1}{k_2} x_1 \tag{14}$$

$$f_{n\ell}(x_1) = \text{sgn}(x_1)\left[\omega\sqrt{2\alpha c|x_1| - \alpha x_1^2} - \frac{1}{k_2}\right]. \tag{15}$$

Note that f_ℓ connects the two disjoint portions of $f_{n\ell}$. Requiring that these two curves be joined continuously with equal slope at $|x_1| = x_\ell$ yields the following k_1 and k_2

$$k_2 = \frac{\sqrt{2\alpha c x_\ell - \alpha x_\ell^2}}{\alpha\omega c x_\ell} \quad \text{and} \quad k_1 = \frac{c - x_\ell}{c x_\ell}. \tag{16}$$

Then, for all of $\mathbb{R}^2$ the control law is

$$u_p(t) = \begin{cases} \text{sat}\big[-k_2 x_2 - k_2 f_p(x_1)\big], & x_1 \in (-2c, 2c) \\ \text{sgn}\big[-x_2 - f_p(x_1)\big], & x_1 \notin (-2c, 2c). \end{cases} \tag{17}$$

For all x outside the region $\mathcal{T}$, the control is equivalent to the time-optimal control in (2). If $x_\ell \to 0$ then $k_2 \to \infty$ and $\frac{1}{k_2} \to 0$ and we recover (2). This control scheme allows us to choose x_ℓ and α though we note that, e.g., choosing k_1 determines k_2 for a given α. We restrict $x_\ell \in [0, \frac{2}{5}c)$ (see Lemma A-2 in the Appendix and Theorem 2 in Section V).

In the following sections, we prove that the control law in (17) leads to a stable closed-loop system. In Section IV, we show that all trajectories will reach $\mathcal{T}$ in finite time. We show in Section V that only the region $\mathcal{B}$ is invariant and in fact the state will exit $\mathcal{T}\backslash\mathcal{B}$. For this case, we show in Section VI that the state will still enter $\mathcal{B}$ in finite time. In Section VII, we show that all states in $\mathcal{B}$ tend asymptotically to the origin by giving a Lyapunov function for $x \in \mathcal{B}$.

IV. All Trajectories Reach $\mathcal{T}$ in Finite Time

For an initial condition x_o, equation (1) is solved by

$$x = \Phi(t - t_o)x_o + \int_0^t \Phi(t - \tau)Bu(\tau)d\tau \tag{18}$$

where the state transition matrix $\Phi(t - \tau)$ is given by

$$\Phi(t - \tau) = \begin{bmatrix} \cos(\omega(t-\tau)) & \frac{\sin(\omega(t-\tau))}{\omega} \\ -\omega\sin(\omega(t-\tau)) & \cos(\omega(t-\tau)) \end{bmatrix}. \tag{19}$$

Noting that the state rotates clockwise at a rate of ω in the phase space, it is trivial to show that given any initial condition in $\mathcal{U}^+$ or $\mathcal{U}^-$, the state reaches the switching curve f_{to} in $t_s \le \frac{\pi}{\omega}$ and the time between subsequent switches is half a period or $\frac{\pi}{\omega}$. A useful property of trajectories subject to f_{to} is that between every switch, the distance of $|x_1|$ to the origin decreases by $2c$ which is illustrated in Figure 2 with trajectories CD and CE [7].

Theorem 1: All trajectories reach $\mathcal{T}$ in finite time.

Proof: Begin by solving (18) for the time it takes the state to cross the x_1-axis from any $x_o = [x_1^o \;\; x_2^o]^T$, e.g., AF in Figure 2. We consider the case where x_o is in the $\mathcal{U}^-$ region. Solving (18) for $x_2 = 0$ at $t = t_1$ gives

$$0 = -\omega x_1^o \sin(\omega t_1) + x_2^o \cos(\omega t_1) - \frac{b_o}{\omega}\sin(\omega t_1). \tag{20}$$

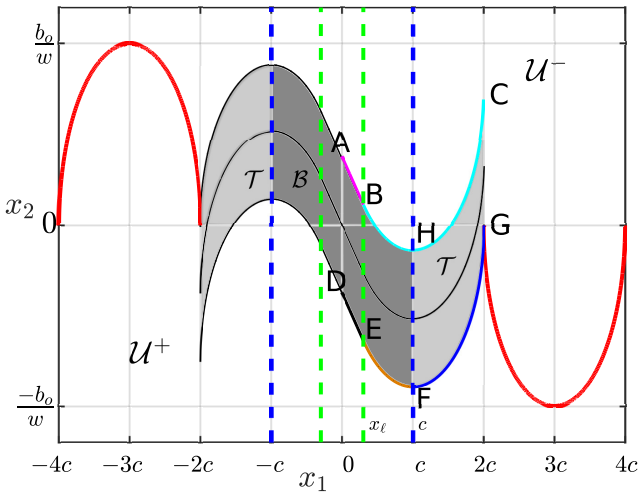

Fig. 3: The entire PTOSω region $\mathcal{T}$ includes both shaded regions, while $\mathcal{B}$ is only the darker shaded region and $\mathcal{T}\backslash\mathcal{B}$ is the lighter shaded region.

Solving (20) for t_1, and using t_1 in row one of (18), we find that

$$x_1(t_1) = \sqrt{\left(\frac{x_2^o}{\omega}\right)^2 + (x_1^o + c)^2} - c. \tag{21}$$

Since the state rotates clockwise, the first switch will occur on the semi-ellipse of the switching curve directly below $x_1(t_1)$. Since at each subsequent switch, the magnitude of x_1 decreases by $2c$, an upper bound on the time $t_\mathcal{T}$ to reach $\mathcal{T}$ is

$$t_\mathcal{T} \le \left[\left\lfloor\left(\frac{x_1(t_1)}{2c}\right)\right\rfloor + 1\right]\frac{\pi}{\omega} < \infty, \quad \forall x_1(t_1) < \infty. \tag{22}$$

■

V. The Region $\mathcal{B}$ is Invariant

In this section, we show that once the state enters the region $\mathcal{B}$, it will remain in $\mathcal{B}$. Consider Figure 3. For $x_1 > 0$, the segments AB and DE represent the upper and lower saturation boundaries of the linear region $\mathcal{L}$, respectively. Similarly, the segments BC and EG represent the upper and lower saturation boundaries of the rest of $\mathcal{T}$. For the state to remain trapped in $\mathcal{T}$ requires that $\text{sgn}(\dot{u}) = -\text{sgn}(u)$ along the upper boundary AC and the lower boundary DG in Figure 3. We will show that this requirement is satisfied for the whole segment AC and along DF but not FG. Hence, $\mathcal{T}\backslash\mathcal{B}$ is not invariant and a state may move freely through the segment FG. For $x \in \mathcal{T}$, the time derivative of $u(t)$ is

$$\dot{u}(t) = f_p'(x_1)u + k_2 f_p'(x_1)f_p(x_1) + k_2\omega^2 x_1 - k_2 b_o u.$$

Denote $u(t)$ at the upper boundary AC as $u_u(t) = -1$, and at the lower boundary DG as $u_\ell(t) = +1$. The requirement that $\text{sgn}(\dot{u}) = -\text{sgn}(u)$ can be expressed as

$$\dot{u}_\ell = f_p'(x_1) + k_2 f_p'(x_1)f_p(x_1) + k_2\omega^2 x_1 - k_2 b_o < 0 \tag{23}$$

$$\dot{u}_u = -f_p'(x_1) + k_2 f_p'(x_1)f_p(x_1) + k_2\omega^2 x_1 + k_2 b_o > 0. \tag{24}$$

We will consider when $x_1 \geq 0$. By anti-symmetry, similar results hold for $x_1 \leq 0$. For $x_1 \geq 0$, we have

$$f_p'(x_1) = \begin{cases} \frac{k_1}{k_2} & 0 \leq x_1 \leq x_\ell \\ \frac{\omega\alpha(c-x_1)}{\sqrt{2\alpha c x_1 - \alpha x_1^2}} & x_\ell < x_1 \leq 2c. \end{cases} \tag{25}$$

Lemma 1: The inequalities (23) and (24) hold in the linear region (on the segments AB and DE).

Proof: Consider first the upper boundary, segment AB, where, using (14) and (25), the inequality in (24) can be written as

$$\frac{k_1}{k_2} < k_2\Big(\frac{k_1}{k_2}\Big)^2 x_1 + k_2\omega^2 x_1 + k_2 b_o.$$

We can make the RHS as small as possible by inserting the smallest possible x_1, i.e., $x_1 = 0$:

$$\frac{k_1}{k_2} < b_o k_2. \tag{26}$$

Now using k_1 and k_2 from (16), we see that

$$\frac{k_1}{k_2^2} = \Big(\frac{c - x_\ell}{c x_\ell}\Big)\frac{\omega^2\alpha^2 c^2 x_\ell^2}{2c\alpha x_\ell - \alpha x_\ell^2} < b_o. \tag{27}$$

Letting $\alpha = 1$ to maximize the LHS, this simplifies to

$$c < 2c,$$

which is clearly always true.

Now consider segment DE, the lower boundary in the linear region, where (23), again for the case $x_1 > 0$, can be written as

$$\Big(\frac{k_1}{k_2}\Big)^2 x_1 + \frac{k_1}{k_2^2} + \omega^2 x_1 < b_o.$$

Now, insert k_1 and k_2 from (16) and maximize the LHS by letting $x_1 = x_\ell$:

$$\frac{(c-x_\ell)^2\omega^2\alpha^2 c^2 x_\ell^2}{c^2 x_\ell^2(2c\alpha x_\ell - \alpha x_\ell^2)} x_\ell + \frac{(c-x_\ell)\omega^2\alpha^2 c^2 x_\ell^2}{c x_\ell(2c\alpha x_\ell - \alpha x_\ell^2)} + \omega^2 x_\ell < b_o$$

$$x_\ell < c$$

which holds by the requirement that $x_\ell < \frac{2}{5}c$. ∎

Lemma 2: Consider the lower boundary in the nonlinear region. Inequality (23) is satisfied for $x_\ell < x_1 < c$, i.e., for the segment EF, but not for $x_1 \geq c$, i.e., segment FG.

Proof: Using (15) and (25), it is easy to show that (23) reduces to

$$c > x_1.$$

∎

Lemma 3: The entire upper boundary AC satisfies (24).

Proof: Since segment AB was already considered in Lemma 1, here we consider only BC. Inserting (15) and (25) into (24) yields

$$0 < \frac{-2\omega\alpha(c-x_1)}{\sqrt{2\alpha c x_1 - \alpha x_1^2}} + k_2\omega^2\alpha c + k_2\omega^2 x_1(1-\alpha) + k_2 b_o. \tag{28}$$

By inspection, the last three terms are positive. However, it is unclear under what condition they will dominate first term when $x_1 < c$, particularly since k_2 depends on our choice of x_ℓ. However, Lemma A-1 in the Appendix states that the RHS of (28) is monotonically increasing with x_1. Hence, we can use the smallest possible value of x_1, that is $x_1 = x_\ell$, to minimize the RHS of (28). Further substituting k_2 from (16), we find after simplification that

$$\begin{aligned} 0 < &-2\omega^2\alpha^2 c(c - x_\ell) + (2\alpha c - \alpha x_\ell)\omega^2\alpha(c - x_\ell) \\ &+ (2\alpha c x_\ell - \alpha x_\ell^2)\omega^2 + (2\alpha c - \alpha x_\ell) b_o. \end{aligned}$$

Now, we make the linear region as small as possible, i.e., let $x_\ell \to 0$ to yield

$$0 < 2\alpha c b_o. \tag{29}$$

Thus, inequality (24) is satisfied over the entire segment AC. ∎

Theorem 2: A state within $\mathcal{B}$ is trapped within $\mathcal{B}$, i.e., $\mathcal{B}$ is invariant.

Proof: By Lemmas 2 and 3, the state will not exit $\mathcal{B}$ via either AH or DF. By requiring that $x_\ell < \frac{2}{5}c$, Lemma A-2 in the Appendix states that for any state on the segment HF, $x_2 < 0$. From (1), this implies that x_1 is *decreasing* and the state is moving toward the interior of $\mathcal{B}$. ∎

VI. All States Enter $\mathcal{B}$ in Finite Time

To show that the state will exit $\mathcal{T}\backslash\mathcal{B}$ and enter $\mathcal{B}$ in finite time, we prove the following lemmas.

Lemma 4: The state exits $\mathcal{T}\backslash\mathcal{B}$ in finite time.

Proof: Assume an initial condition x_o on segment HC, i.e., the upper saturation boundary between $(c, 2c]$. Now, suppose $u = +1$ and call the resulting trajectory $x_{u^+}(t)$ which achieves a minimum at $t_m \leq \frac{\pi}{\omega}$ when $\dot{x}_{2,u^+} = 0$. Considering (1), this means

$$x_{1,u^+}(t_m) = c.$$

Now, consider $x_p(t_m)$, the trajectory from the same x_o but under the PTOSω control. We would like to show that at t_m, $x_{1,u^+}(t_m) \geq x_{1,p}(t_m)$. Using the x_1-component of (18), this is equivalent to

$$\int_0^{t_m} \frac{b_o}{\omega}\sin\big(\omega(t_m - \tau)\big)(1 - u_p(\tau))d\tau \geq 0.$$

Since $\sin\xi \geq 0$, $\xi \in [0, \pi]$ and $|u_p(t)| \leq 1$, this convolution is non-negative. Equivalently then

$$x_{1,p}(t_m) \leq x_{1,u^+}(t_m) = c, \tag{30}$$

which implies that $x_{1,p}(t_m) \notin \mathcal{T}\backslash\mathcal{B}$. Furthermore, we showed in Lemma 3 that a trajectory will not exit $\mathcal{T}$ via segment AC. Therefore, $x_p(t_m) \in \mathcal{U}^+ \cup \mathcal{B}$. Thus, the state must exit $\mathcal{T}\backslash\mathcal{B}$ via either HF, CG, or FG. ∎

Lemma 5: If the state exits $\mathcal{T}$ along FG with $x = [c + \beta, x_2^{exit}]^T$, where $\beta \in (0, c]$, (illustrated as "trajectory 3" in Figure 4), then the state will enter $\mathcal{B}$ with $x_1 \geq c - \beta$ and $x_2^{entry} \leq x_2^{exit}$. Equality holds when $c - \beta \geq x_\ell$.

Proof: Suppose the state exits $\mathcal{T}$ with $x = [c + \beta, x_2^{exit}]^T$. Recalling that the mass of the system is $\frac{1}{b_o}$ and the spring constant is $\frac{1}{c}$, we find that the total energy (kinetic and potential), T, of the system at this point is

$$T = \frac{1}{2c}(c+\beta)^2 + \frac{1}{2b_o}(x_2^{exit})^2. \tag{31}$$

Now assume $u(t) = 1$ over an interval from $x_1 = c + \beta$ to $x_1 = c - \beta$. Integrating $u(t)$ over this interval yields the work done by the control,

$$W_u = \int_{c+\beta}^{c-\beta} (1) dx_1 = -2\beta. \tag{32}$$

Now consider the change in potential energy of the spring due to the same change in x_1,

$$\Delta T_s = \frac{1}{2c}(c-\beta)^2 - \frac{1}{2c}(c+\beta)^2 = -2\beta.$$

Hence, after the state has traversed a distance $\Delta x_1 = 2\beta$, by conservation of energy, we must have $x_2^{exit} = x_2^{entry}$. Since the nonlinear portion of the lower boundary is symmetric about c, the state enters $\mathcal{B}$ precisely at $x = [c-\beta,\, x_2^{exit}]^T$ if $c - \beta \geq x_\ell$. If $c - \beta < x_\ell$, the trajectory intercepts the linear region of $\mathcal{B}$ with $x_1 > c - \beta$ and $x_2 < x_2^{exit}$, i.e., *before* $x = [c-\beta,\, x_2^{exit}]^T$.

Furthermore, the time for this to occur is bounded by $t < \frac{\pi}{\omega}$ since such trajectories are less than a half rotation. ■

Lemma 6: Suppose the state exits $\mathcal{T}$ via the segment CG. Then the state will enter $\mathcal{B}$ in $t \leq \frac{2\pi}{\omega}$.

Proof: Since the x_2-component of a state along CG is positive, x_1 is increasing and the state exits $\mathcal{T}$. When a state exits via CG, it re-enters the time-optimal region $\mathcal{U}^-$and will cross the x_1-axis with $x_1 \in (2c, 4c]$. Using (21), an upper bound on x_1 at the crossing can be found by considering an x_o at point C or $x_o = [2c,\, \frac{2}{k_2}]^T$ in (21). Using $x_\ell = \frac{2}{5}c$ and $\alpha = 1$ maximizes x_2^o to be ωc. Equation (21) then gives

$$x_1(t_1) = c(\sqrt{10} - 1). \tag{33}$$

This means that at the end of the *next* switch, $|x_1| \leq x_1(t_1) - 2c < c$ so the time for the state to exit $\mathcal{T}$ via CG and enter $\mathcal{B}$ is bounded by $t < \frac{2\pi}{\omega}$. ■

Theorem 3: All states enter $\mathcal{B}$ in finite time.

Proof: By Theorem 1, all states enter $\mathcal{T}$ in finite time. By Lemma 4, all states that enter $\mathcal{T}\backslash\mathcal{B}$ will exit $\mathcal{T}\backslash\mathcal{B}$ in less than half a period. Lemmas 5 and 6 show that a state that exits $\mathcal{T}\backslash\mathcal{B}$ and enters $\mathcal{U}^+$ or $\mathcal{U}^-$ will enter $\mathcal{B}$ in less than one period. Hence, a (very loose) upper bound on the time, $t_\mathcal{B}$, for a state to reach $\mathcal{B}$ upon entering $\mathcal{T}\backslash\mathcal{B}$ is given by $t_\mathcal{B} < \frac{3\pi}{\omega}$. ■

VII. $\mathcal{B}$ Is Asymptotically Stable In The Sense of Lyapunov

We have shown that all states will become trapped within $\mathcal{B}$. Now, we show that for $x \in \mathcal{B}$, x tends asymptotically to the origin. We do this by determining a Lyapunov function $V(x)$ for the Region $\mathcal{B}$.

Define the Lyapunov candidate function $V(x)$ as

$$V(x) \coloneqq \frac{1}{2}x_2^2 + \int_0^{x_1} p(s)ds, \tag{34}$$

$$p(x_1) \coloneqq \omega^2 x_1 + b_o k_2 f_p(x_1). \tag{35}$$

To show that (34) is a Lyapunov function, we prove the following lemmas.

Lemma 7: $V(x)$ is positive-definite $\forall x \in \mathcal{B}$.

Proof: Clearly, $\frac{1}{2}x_2^2 \geq 0$. Furthermore, by Lemma (A-3), $p(-x_1) = -p(x_1)\ \forall x_1 \in \mathcal{B}$ and $p(x_1) \geq 0$ for $x_1 \geq 0$. This implies that $\int_0^{\pm x_1} p(s)ds > 0$. Therefore, $V(x) \geq 0 \quad \forall x \in \mathcal{B}$.

Furthermore, since we have just shown that both terms of $V(x)$ are positive, it is a trivial observation that $V(x) = 0 \iff x = 0$ ■

Lemma 8: $\dot{V}(x)$ is negative-definite $\forall x \in \mathcal{B}$.

Proof: Differentiating (34) yields

$$\dot{V}(x) = -b_o k_2 x_2^2 \leq 0, \ \forall x \in \mathcal{B}. \tag{36}$$

Clearly, (36) is negative semi-definite for all $x \in \mathcal{B}$. Furthermore, suppose $x = 0$. Then by inspection, $\dot{V}(0) = 0$.

Now, suppose $\dot{V}(x) = 0$. Then it must be that $x_2 = 0$. Thus when $\dot{V}(0) = 0$, possible solutions to (1) must have the form $[x_1, 0]^T$. Hence, $x_2 = 0$ which implies that

$$\dot{x}_2 = 0 = -\omega^2 x_1 - b_o k_2 f_p(x_1). \tag{37}$$

Now $f_p(x_1) = 0 \iff x_1 = 0$, $x \in \mathcal{B}$ (recall the linear region through the origin). By Lemma A-3, x_1 and $f_p(x_1)$ always have the same sign. Thus, (37) is only satisfied if

$$\omega^2 x_1 = -b_o k_2 f(x_1) = 0 \implies x_1 = 0. \tag{38}$$

Therefore, $\dot{V}(x)$ is negative-definite. ■

VIII. Results

We simulated the PTOSω controller in SIMULINK using $b_o = 1.8276 \times 10^7$ and $\omega = 1.9949 \times 10^3$ rad/s which are representative of a simplified AFM model [3]. We chose an initial condition of $x = [3c,\, 0]^T$.

Using the PTOSω controller, we simulated both the ideal plant and a plant where b_o is increases by 5% and ω is decreased by 5%. The size of the linear region is $x_\ell = 0.1c$ and $\alpha = 0.8$. We used a fixed time step of 1×10^{-9} s for all simulations. These results are shown in Figure 5. The solid green curve represents a trajectory where we assume a perfect model, while the dashed blue curve represents the imperfect model. Figure 6 shows the control history of the PTOSω controller which clearly demonstrates the success of the method. Note how the PTOSω controller in Figure 6 smoothly brings both systems to the origin free of any chattering in the control signal.

IX. Conclusions and Future Work

We have developed a near time-optimal control law, the PTOSω, for a second-order oscillator system. We have shown that this control law leads to a stable closed-loop system under certain design constraints. However, we note that we have developed this law for a system with zero damping and only as a regulator. To make a control law which is more realistically applicable, future work will build on this development to construct a similar control law for set point tracking of systems with damping. Future work will also seek experimental validation through implementing these PTOSw controllers on an actual AFM.

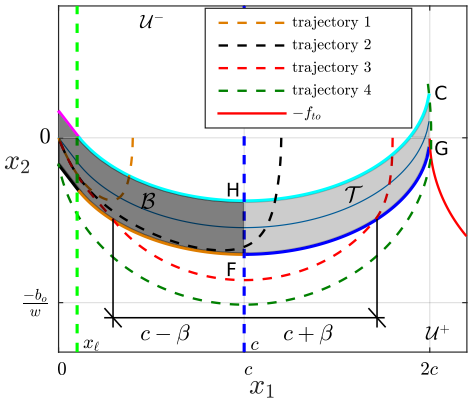

Fig. 4: Plot showing possibilities of how the state enters $\mathcal{B}$.

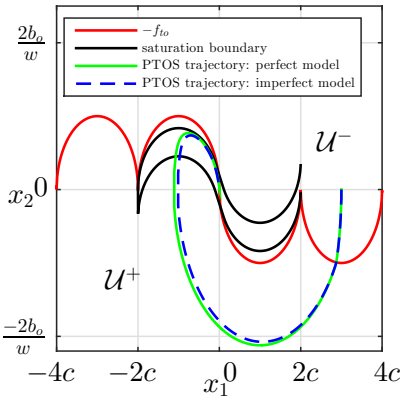

Fig. 5: Trajectories under the PTOSω control law for a plant with perfectly known parameters and with 5% parameter variation.

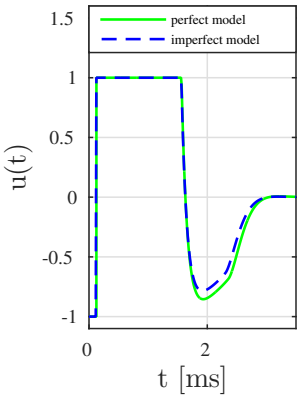

Fig. 6: Control histories of the PTOSω controller.

REFERENCES

[1] J. Butterworth, L. Y. Pao, and D. Abramovitch, "Dual-adaptive feedforward control for raster tracking with applications to AFMs," in *Control Applications (CCA), 2011 IEEE International Conference on*, Sept 2011, pp. 1081–1087.

[2] S. Salapaka, A. Sebastian, J. P. Cleveland, and M. V. Salapaka, "High bandwidth nano-positioner: A robust control approach," *Review of Scientific Instruments*, vol. 73, no. 9, pp. 3232–3241, 2002.

[3] S. Andersson and L. Pao, "Non-raster sampling in atomic force microscopy: A compressed sensing approach," in *American Control Conference (ACC), 2012*, June 2012, pp. 2485–2490.

[4] E. Candes and M. Wakin, "An introduction to compressive sampling," *Signal Processing Magazine, IEEE*, vol. 25, no. 2, pp. 21–30, March 2008.

[5] A. Bryson and Y. Ho, *Applied Optimal Control*. Hemisphere Publishing Corporation, 1975.

[6] Z. Shen, P. Huang, and S. B. Andersson, "Calculating switching times for the time-optimal control of single-input, single-output second-order systems," *Automatica*, vol. 49, no. 5, pp. 1340 – 1347, 2013.

[7] E. P. Ryan, *Optimal Relay and Saturating Control System Synthesis*. Peter Peregrinus, 1982.

[8] R. Oldenburger and G. Thompson, "Introduction to time optimal control of stationary linear systems," *Automatica*, vol. 1, no. 23, pp. 177 – 205, 1963.

[9] M. Athans and P. L. Falb, *Optimal Control*. Mineola, New York: Dover Publications, Inc., 2007.

[10] W. Newman, "Robust near time-optimal control," *Automatic Control, IEEE Transactions on*, vol. 35, no. 7, pp. 841–844, Jul 1990.

[11] M. Workman, "Adaptive Proximate Time-Optimal Servomechanisms," Ph.D. dissertation, Stanford University, Stanford, CA, March 1987.

[12] L. Pao and G. Franklin, "Proximate time-optimal control of third-order servomechanisms," *Automatic Control, IEEE Transactions on*, vol. 38, no. 4, pp. 560–580, Apr 1993.

[13] J. L. Junkins and Y. Kim, *Introduction to Dynamics and Control of Flexible Structures*. Washington, DC: American Institute of Aeronautics and Astronautics, Inc., 1993.

[14] G. F. Franklin, J. D. Powell, and M. Workman, *Digital Control of Dynamic Systems*. Half Moon Bay, CA: Ellis-Kagle Press, 1998.

APPENDIX

Lemma A-1: On the upper saturation boundary BC, the RHS of (28), which we call $\dot{u}_u((x_1(t))$, is monotonically increasing with x_1.

Proof: To show this, we will show that $\frac{d}{dx_1}\dot{u}_u(x_1) > 0$ over the entire interval, $x_1 \in [x_\ell, 2c]$. Calculating the derivative, we see that

$$\frac{d}{dx_1}\dot{u}_u(x_1) = \frac{2\omega\alpha}{\sqrt{2\alpha c x_1 - \alpha x_1^2}} + \frac{2\omega\alpha^2(c-x_1)^2}{(2\alpha c x_1 - \alpha x_1^2)^{3/2}} + k_2\omega^2(1-\alpha) > 0. \quad \text{(A-1)}$$

holds for $x \in [x_\ell,\ 2c]$ and $\alpha \in (0,\ 1]$. ■

Lemma A-2: Call the upper saturation boundary $f_u(x_1) = -f_{n\ell}(x_1) + \frac{1}{k_2}$. Then, $f_u(c) < 0\ \forall |x_\ell| < \frac{2}{5}c$.

Proof: Along the upper saturation boundary, $u(t) = -1$, so at $x_1 = c$, we have

$$u = -1 = -k_2 f_p(c) - k_2 x_2. \quad \text{(A-2)}$$

Requiring that $x_2 < 0$ gives

$$x_2 = \frac{2}{k_2} - \omega c\sqrt{\alpha} < 0. \quad \text{(A-3)}$$

Inserting k_2 from (16), yields $x_\ell < \frac{2}{5}c$. ■

Lemma A-3: Let $p(x_1)$ be given by (35). Then $p(x_1)x_1 > 0,\ x \in \mathcal{B}$.

Proof: In other words, $p(x_1)$ is an odd function and positive for $x_1 > 0$. Clearly, this is true for the $\omega^2 x_1$ term of (35). Furthermore, by inspection, this is also true for $f_\ell(x_1)$ in (14). Now, we show that $f_{n\ell}(x_1) > 0,\ x_1 \in \mathcal{B}\backslash\mathcal{L}$, where $f_{n\ell}$ is given (15). We want, i.e., that

$$\omega\sqrt{2\alpha c|x_1| - \alpha x_1^2} > \frac{\omega\alpha c x_\ell}{\sqrt{2\alpha c x_\ell - \alpha x_\ell^2}}. \quad \text{(A-4)}$$

Now, recalling that $x_1 \le c, \forall x_1 \in \mathcal{B}$ we make the LHS as small as possible by letting $x_1 = x_\ell$. Easy simplifications yield $c > x_\ell$ which holds since we require $x_\ell < \frac{2}{5}c$. To see that $f_p(x_1) < 0$ for $x_1 < -x_\ell$, note that the sgn$(\cdot)$ in (15) will flip the inequality and we will have again (A-4). Thus, $f_p(x_1)$ is an odd function , and positive for positive x_1. ■